DIRECT NUMERICAL SIMULATION OF TURBULENCE USING SYMMETRY-PRESERVING DISCRETIZATION

R.W.C.P. VERSTAPPEN AND A.E.P. VELDMAN
Research Institute for Mathematics and Computing Science, University of Groningen
P.O.Box 800, 9700 AV Groningen, The Netherlands
e-mail: verstappen@math.rug.nl, veldman@math.rug.nl

Abstract. We propose to perform turbulent flow simulations in such a manner that the difference operators do have the same symmetry properties as the underlying differential operators, *i.e.* the convective operator is represented by a skew-symmetric matrix and the diffusive operator is approximated by a symmetric, positive-definite matrix. Such a symmetry-preserving discretization of the Navier-Stokes equations is stable on any grid, and conserves the total mass, momentum and kinetic energy (when the physical dissipation is turned off). Its accuracy is tested for a turbulent channel flow at Re=5,600 (based on the channel width and the mean bulk velocity) by comparing the results to those of physical experiments and previous numerical studies. This comparison shows that with a fourth-order, symmetry-preserving method a $64 \times 64 \times 32$ grid suffices to perform an accurate direct numerical simulation.

1. Introduction

The smallest scales of motion in a turbulent flow result from a subtle balance between convective transport and diffusive dissipation. In mathematical terms, the balance is an interplay between two differential operators differing in symmetry: the convective derivative is skew-symmetric, whereas diffusion is governed by a symmetric, definite operator. With this in mind, we have developed a spatial discretization method which preserves the symmetries of the balancing differential operators. That is, convection is approximated by a skew-symmetric discrete operator, and diffusion is discretized by a symmetric, definite operator. Second-order and fourth-order

versions have been developed thus far, applicable to structured nonuniform grids. The resulting semi-discrete representation conserves energy exactly in the absence of physical dissipation. For finite Reynolds numbers, *i.e.* in the presence of physical dissipation, the kinetic energy of any discrete solution decreases unconditionally in time. Therefore, a symmetry-preserving, spatial discretization is stable on any grid, and we need not add an artificial demping mechanism that will inevitably interfere with the subtle balance between convection and diffusion at the smallest length scales. This forms our motivation to investigate symmetry-preserving discretizations for direct numerical simulation (DNS) of turbulent flow. Because stability is not an issue, the main question becomes how accurate is a symmetry-preserving discretization, or stated otherwise, how coarse may the grid be for a DNS? We will address this question in Section 2 by evaluating the results for a turbulent flow in a channel at Re=5,600. We will kick off by sketching the main lines of symmetry-preserving discretization (Section 1). For a more detailed discussion, we refer to Verstappen and Veldman (1998, 2002). Conservation properties of numerical schemes for the Navier-Stokes equations are currently also pursued at other research institutes, see e.g. Hyman *et al.* (1992), Morinishi *et al.* (1998), Vasilyev (2000), Twerda (2000) and Ducros *et al.* (2000).

2. Symmetry-preserving discretization

The temporal evolution of the discrete velocity vector $\boldsymbol{u}_h$ is governed by a finite-volume discretization of the incompressible Navier–Stokes equations:

$$\boldsymbol{\Omega}\frac{\mathrm{d}\boldsymbol{u}_h}{\mathrm{d}t} + \boldsymbol{C}(\boldsymbol{u}_h)\,\boldsymbol{u}_h + \boldsymbol{D}\boldsymbol{u}_h - \boldsymbol{M}^*\boldsymbol{p}_h = \boldsymbol{0} \qquad \boldsymbol{M}\boldsymbol{u}_h = \boldsymbol{0}, \tag{1}$$

where the vector $\boldsymbol{p}_h$ denotes the discrete pressure, $\boldsymbol{\Omega}$ is a (positive-definite) diagonal matrix representing the sizes of the control volumes, $\boldsymbol{C}(\boldsymbol{u}_h)$ is built from the convective flux contributions through the control faces, $\boldsymbol{D}$ contains the diffusive fluxes, and $\boldsymbol{M}$ is the coefficient matrix of the discretization of the integral form of the law of conservation of mass. The coefficient matrices $\boldsymbol{C}(\boldsymbol{u}_h)$ and $\boldsymbol{D}$ are constructed such that

$$\boldsymbol{C}(\boldsymbol{u}_h) + \boldsymbol{C}^*(\boldsymbol{u}_h) = \boldsymbol{0}, \qquad \boldsymbol{D} + \boldsymbol{D}^* \text{ positive-definite.} \tag{2}$$

The symmetry condition on the coefficient matrix $\boldsymbol{C}(\boldsymbol{u}_h)$ reflects that $\boldsymbol{C}(u_h)$ represents a discrete gradient operator: its null space consists of the constant vectors (provided that the consistency condition $\boldsymbol{C}(\boldsymbol{u}_h)\,\boldsymbol{1} = \boldsymbol{0}$ is satisfied) and $\boldsymbol{C}(\boldsymbol{u}_h)$ is skew-symmetric like a first-order differential operator. The coefficient matrix $\boldsymbol{D}$ of the discrete diffusive operator inherits its positive-definiteness from the underlying diffusive, differential operator $-\nabla\cdot\nabla/\mathrm{Re}$.

The semi-discretization (1)–(2) is conservative and stable. The total mass is trivially conserved, and the same holds for the total amount of momentum (provided that the discretization is exact for $\boldsymbol{u}_h = \mathbf{1}$). The evolution of the discrete energy $\boldsymbol{u}_h^* \boldsymbol{\Omega} \boldsymbol{u}_h$ of any solution $\boldsymbol{u}_h$ of (1)–(2) is governed by

$$\begin{aligned} \frac{\mathrm{d}}{\mathrm{d}t}(\boldsymbol{u}_h^* \boldsymbol{\Omega} \boldsymbol{u}_h) &\overset{(1)}{=} -\boldsymbol{u}_h^*(\boldsymbol{C} + \boldsymbol{C}^*)\boldsymbol{u}_h - \boldsymbol{u}_h^*(\boldsymbol{D} + \boldsymbol{D}^*)\boldsymbol{u}_h + \underbrace{2\boldsymbol{p}_h^* \boldsymbol{M} \boldsymbol{u}_h}_{=0} \\ &\overset{(2)}{=} -\boldsymbol{u}_h^*(\boldsymbol{D} + \boldsymbol{D}^*)\boldsymbol{u}_h \leq 0, \end{aligned} \tag{3}$$

where we have used the skew-symmetry of $\boldsymbol{C}(\boldsymbol{u}_h)$. The right-hand side is zero if and only if $\boldsymbol{u}_h = \mathbf{0}$, or $\boldsymbol{D} + \boldsymbol{D}^* = \mathbf{0}$. Thus, the energy is conserved if the diffusion is turned off. Note that the pressure term $\boldsymbol{M}^* \boldsymbol{p}_h$ in (1) does not affect the evolution of the total kinetic energy (on condition that $\boldsymbol{M}\boldsymbol{u}_h = \mathbf{0}$), because the discrete pressure gradient is represented by the transpose of the coefficient matrix $\boldsymbol{M}$ of the incompressibility constraint.

With diffusion (that is for $\boldsymbol{D} \neq \mathbf{0}$) the right-hand side of (3) is negative for all $\boldsymbol{u}_h \neq \mathbf{0}$ provided that $\boldsymbol{D} + \boldsymbol{D}^*$ is positive-definite. So, the energy of the discrete system (1) decreases in time if (2) is satisfied. The semi-discrete system (1) is stable under this symmetry condition: a solution of (1) can be obtained on any grid, and there is no need to add an artificial damping mechanism to stabilize the spatial discretization.

Since these favorable conservation and stability properties are directly related to the symmetries of the coefficient matrices in (1), we want to construct these matrices such that they fulfil (2). To illustrate the way in which this may be achieved, we consider the approximation of the first-order derivative in one spatial dimension. The traditional method maximizes the (formal) order of the local truncation error. On a stencil consisting of three points, this leads to the second-order approximation

$$\partial_x u(x_i) \approx \tfrac{1}{2}\Omega_i^{-1}\left(r_i^{-1}u_{i+1} - (r_i^{-1} - r_i)u_i - r_i u_{i-1}\right), \tag{4}$$

where

$$\Omega_i^{-1} = \tfrac{1}{2}\left(x_{i+1} - x_{i-1}\right) \qquad \text{and} \qquad r_i = (x_{i+1} - x_i)/(x_i - x_{i-1}).$$

The essence of our method is that the first-order derivative $\partial_x u(x_i)$ is approximated by a discrete operator $\boldsymbol{\Omega}^{-1}\boldsymbol{C}$, where the coefficient matrix $\boldsymbol{C}$ is skew-symmetric:

$$\partial_x u(x_i) \approx \tfrac{1}{2}\Omega_i^{-1}\left(u_{i+1} - u_{i+1}\right). \tag{5}$$

The two ways of discretization are illustrated in Figure 1.

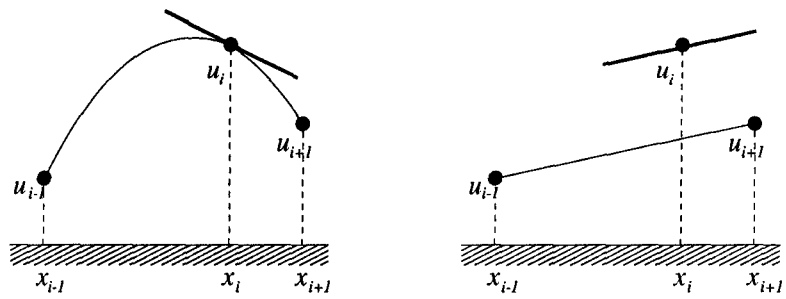

Figure 1. Two ways of approximating $\partial_x u$. In the left-hand figure the derivative is approximated by means of a Lagrangian interpolation, that is by Eq. (4). In the right-hand figure the symmetry-preserving discretization (5) is applied.

As the diagonal-entry of operator in the right-hand side of (4) is non-zero for $r_1 \neq 1$, the standard discretization method breaks the skew-symmetry on a nonuniform grid. Consequently, the standard method does not conserve the energy and is not conditionally stable on nonuniform meshes.

The local truncation error of the symmetry-preserving discretization

$$\tau_h(x_i) = \tfrac{1}{2}(\delta x_{i+1} - \delta x_i)\partial_{xx}u(x_i) + \mathcal{O}(\delta x_{\max}^2), \tag{6}$$

is first-order, unless the grid is (almost) uniform. Given stability, a sufficient condition for second-order accuracy of the discrete solution u_i is that the local truncation error $\boldsymbol{\tau}_h$ be second order. Then the error $\boldsymbol{\epsilon}_h$ in the solution $\boldsymbol{u}_h$, given by $\boldsymbol{\Omega}^{-1}\boldsymbol{C}\boldsymbol{\epsilon}_h = \boldsymbol{\tau}_h$, is second-order. Yet, this is not a necessary condition, as is emphasized by Manteufel and White (1986). They have proven that the symmetry-preserving approximation yields second-order accurate solutions on uniform as well as on nonuniform meshes, even though its local truncation error $\boldsymbol{\tau}_h$ is formally only first-order on nonuniform meshes.

The accuracy of the basic scheme (5) may be improved by means of a Richardson extrapolation, just like in Antonopoulos-Domis (1981). This results into the following, fourth-order accurate discretization:

$$\partial_x u(x_i) \approx \tfrac{1}{2}\Omega_i^{-1}\left(-u_{i+2} + 8u_{i+1} - 8u_{i-1} + u_{i-2}\right),$$

where

$$\Omega_i = \tfrac{1}{2}\left(-x_{i+2} + 8x_{i+1} - 8x_{i-1} + x_{i-2}\right).$$

The diffusive operator undergoes a similar treatment, leading to

$$\Omega_i \partial_{xx}u(x_i) = 8\left(\frac{u_{i+1}-u_i}{x_{i+1}-x_i} - \frac{u_i - u_{i-1}}{x_i - x_{i-1}}\right) - \left(\frac{u_{i+2}-u_i}{x_{i+2}-x_i} - \frac{u_i - u_{i-2}}{x_i - x_{i-2}}\right).$$

Next, we will compare the symmetry-preserving discretization with the traditional discretization methods based on Lagrange interpolation (minimizing local truncation error) for a steady-state solution of the convection-diffusion equation

$$\partial_t u + \bar{u}\partial_x u - \partial_{xx} u/\mathrm{Re} = 0.$$

Since on uniform grids the methods are equal, we choose an example with a boundary-layer character, requiring grid refinement near the outflow boundary $x = 1$. This is achieved by imposing the boundary conditions $u(0,t) = 0$ and $u(1,t) = 1$. The parameters are set equal to $\bar{u} = 1$ and $\mathrm{Re} = 1,000$.

Grid refinement has been carried out on an exponentially stretched grid, with half the grid points in the thin boundary layer of thickness $10/\mathrm{Re}$ near $x = 1$. Four discretization methods have been investigated:

- The traditional Lagrangian second-order method (2L) and its fourth-order counterpart (denoted by 4L) where we have implemented exact boundary conditions to circumvent the problem of a difference molecule that is too large near the boundary;
- The second-order (2S) and fourth-order (4S) symmetry-preserving methods.

We form the vector $\boldsymbol{u}_{\mathrm{exact}}$ by restricting the analytical solution to the grid points, and monitor the global discretization error defined by $||\boldsymbol{u}_h - \boldsymbol{u}_{\mathrm{exact}}||_h$ (where the norm is the kinetic energy norm). Figure 2 shows the global error as a function of the mean mesh size $1/N$, where N is the number of grid points.

A number of observations can be made.

- For all grid sizes the Lagrangian discretization appears to be less accurate than its symmetry-preserving alternative.
- For coarser grids the 4th-order Lagrangian method is not even as accurate as its 2nd-order Lagrangian relative. Similar observations have been made frequently, and this explains why thusfar 4th-order discretization has not been very popular.
- The symmetry-preserving methods already behave nicely on coarse grids. They display a regular monotone behaviour upon grid refinement. Moreover, the discretization error of 4S (2S) picks up its final slope at much coarser grids then 4L (2L). As in turbulent-flow simulations one will always have to cope with limitations on the affordable number of grid points, methods that are less sensitive in this respect are preferable.
- Also note that for a given accuracy (say 10^{-5}), the grid size of the 4th-order symmetry-preserving method can be chosen roughly three times larger than that of the 4th-order Lagrangian method!

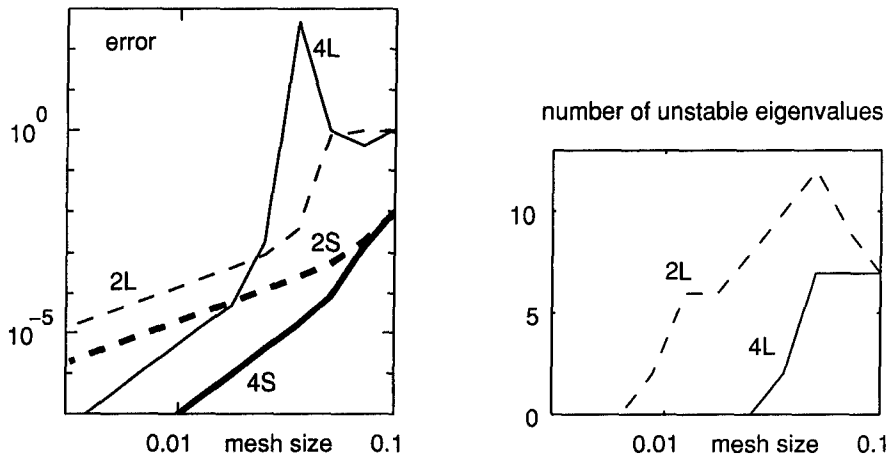

Figure 2. The left-hand figure shows the global error as a function of the mean mesh size on an exponential grid with half of the grid points inside a boundary layer of thickness 10/Re. Four methods are shown: 2L and 4L (2nd- and 4th-order Lagrangian), 2S and 4S (2nd- and 4th-order symmetry-preserving). The right-hand figure depicts the number of eigenvalues of the Lagrangian methods 2L and 4L located in the unstable halfplane. Only the Lagrangian methods are shown, since the symmetry-preserving discretization keeps all the eigenvalues in the stable halfplane.

– The fourth-order Lagrangian method nearly breaks down for $N = 28$ where the stretching factor is 0.72 (which is not extreme). This is due to an eigenvalue moving from the unstable half plane (for low values of N), towards the stable half plane (for higher N), which crosses the imaginary axis close to the origin, making the coefficient matrix almost singular. When one or more eigenvalues of the coefficient matrix are located in the unstable halfplane, the corresponding time-dependent, semi-discrete system is unstable, and can not be integrated in the time domain. In the above examples we have computed the discrete steady-state by a direct matrix solver to avoid this problem.

For details concerning the application to the three-dimensional, incompresible Navier-Stokes equation, we refer to Verstappen and Veldman (1998, 2002). On a uniform grid, the second order scheme proposed by Harlow and Welsh (1965) preserves the symmetries of the convective and diffusive operator. In outline, we have generalized Harlow and Welsh's scheme to nonuniform meshes in such a manner that the symmetries are not broken, and apply Richardson extrapolation to improve the order of accuracy. A variant of our approach for collocated grids has been developed at Delft University (Twerda, 2000).

3. A challenging test-case: turbulent channel flow

In this section, the symmetry-preserving discretization is tested for turbulent channel flow. The Reynolds number is set equal to Re = 5,600 (based on the channel width and the bulk velocity), a Reynolds number at which direct numerical simulations have been performed by several research groups; see Kim *et al.* (1987), Gilbert and Kleiser (1991), Kuroda *et al.* (1995). In addition we can compare the numerical results to experimental data from Kreplin and Eckelmann (1979).

As usual, the flow is assumed to be periodic in the stream- and spanwise direction. Consequently, the computational domain may be confined to a channel unit of dimension $2\pi \times 1 \times \pi$, where the width of the channel is normalized. All computations presented in this section have been performed with 64 (uniformly distributed) streamwise grid points and 32 (uniformly distributed) spanwise points. In the lower-half of the channel, the wall-normal grid points are computed according to

$$y_j = \frac{\sinh(\gamma j/N_y)}{2\sinh(\gamma/2)} \qquad \text{with} \quad j = 0, 1, ..., N_y/2,$$

where N_y denotes the number of grid points in the wall-normal direction. The stretching parameter γ is taken equal to 6.5. The grid points in the upper-half are computed by means of symmetry.

The temporal integration of (1) is performed with the help of a one-leg method that is tuned to improve its convective stability (Verstappen and Veldman, 1997). The non-dimensional time step is set equal to $\delta t = 1.25\ 10^{-3}$. Mean values of computational results are obtained by averaging the results over the directions of periodicity, the two symmetrical halves of the channel, and over time. The averaging over time starts after a start-up period. The start-up period as well as the time-span over which the results are averaged, 1500 non-dimensional time-units, are identical for all the results shown is this section. Figure 3 shows a comparison of the mean velocity profile as obtained from our fourth-order symmetry-preserving simulation ($N_y = 64$) with those of other direct numerical simulations. Here it may be stressed that the grids used by the DNS's that we compare with have typically about 128^3 grid points, that is 16 times more grid points than our grid has. Nevertheless, the agreement is excellent.

To investigate the convergence of the fourth-order method upon grid refinement, we have monitored the skin friction coefficient C_f as obtained from simulations on four different grids. We will denote these grids by A, B, C and D. Their spacings differ only in the direction normal to the wall. They have $N_y = 96$ (grid A), $N_y = 64$ (B), $N_y = 56$ (C) and $N_y = 48$ (D) points in the wall-normal direction, respectively. The first (counted from

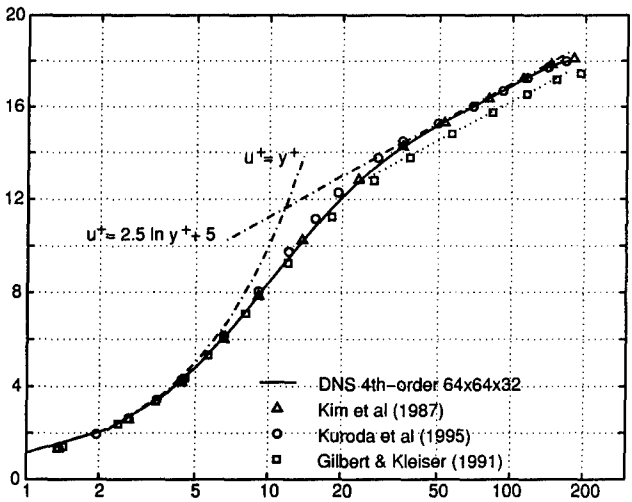

Figure 3. The mean streamwise velocity u^+ versus y^+. The dashed lines represent the law of the wall and the log law. The markers represent DNS-results that are taken from the ERCOFTAC Database.

the wall) grid line used for the convergence study is located at $y_1^+ \approx 0.95$ (grid A), $y_1^+ \approx 1.4$ (B), $y_1^+ \approx 1.6$ (C), and $y_1^+ \approx 1.9$ (D), respectively. Figure 4 displays the skin friction coefficient C_f as function of the fourth

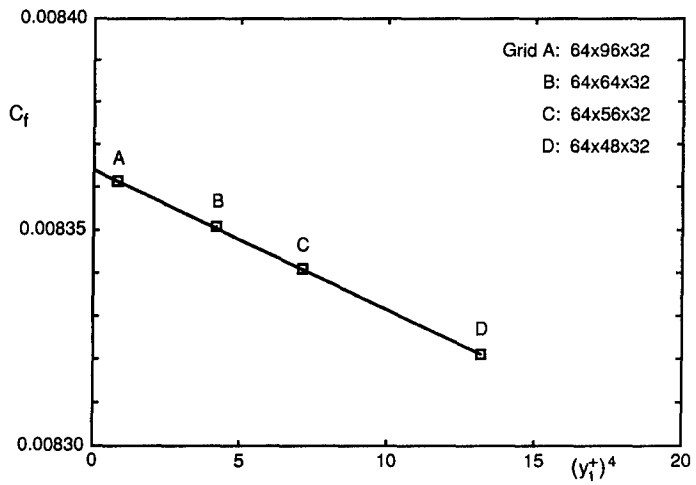

Figure 4. Convergence of the skin friction coefficient C_f upon grid refinement. The figure displays C_f versus the fourth power of the first grid point y_1^+.

power of y_1^+. The convergence study shows that the discretization scheme is indeed fourth-order accurate (on a nonuniform mesh). This indicates that the underlying physics is resolved when 48 or more grid points are used in the wall normal direction. In terms of the local grid spacing (measured by y_1^+), the skin friction coefficient is approximately given by $C_f = 0.00836 - 0.000004(y_1^+)^4$. The extrapolated value at $y_1^+ = 0$ lies in between the C_f reported by Kim *et al.* (1987) ($C_f = 0.00818$) and Dean's correlation of $C_f = 0.073\ Re^{-1/4} = 0.00844$ (Dean, 1978).

The convergence of the fluctuating streamwise velocity near the wall ($0 < y^+ < 20$) is presented in Figure 5. Here, we have added results obtained on three still coarser grids (with $N_y = 32$, $N_y = 24$ and $N_y = 16$ points in the wall-normal direction, respectively), since the results on the grids A, B, C and D fall almost on top of each other. The coarsest grid, with only $N_y = 16$ points to cover the channel width, is coarser than most of the grids used to perform a large-eddy simulation (LES) of this turbulent flow. Nevertheless, the $64 \times 16 \times 32$ solution is not that far off the solution on finer grids, in the near wall region. Further away from the wall, the turbulent fluctuations predicted on the coarse grids ($N_y \leq 32$) become too high compared to the fine grid solutions, as is shown in Figure 6.

The solution on the $64 \times 24 \times 32$, for example, forms an excellent starting point for a large-eddy simulation. The root-mean-square of the fluctuating streamwise velocity is not far of the fine grid solution, and viewed through physical glasses, the energy of the resolved scales of motion, the coarse grid ($N_y = 24$) solution, is convected in a stable manner, because it is conserved by the discrete convective operator. Therefore, we think that the symmetry-preserving discretization forms a solid basis for testing sub-grid scale models. The discrete convective operator transports energy from a resolved scale of motion to other resolved scales without dissipating any energy, as it should do from a physical point of view. The test for a sub-grid scale model then reads: does the addition of the dissipative sub-grid model to the conservative convection of the resolved scales reduce the error in the computation of u_{rms}.

The results for the fluctuating streamwise velocity u_{rms} are compared to the experimental data of Kreplin and Eckelmann (1979) and to the numerical data of Kim *et al.* (1987) in Fig. 7. This comparison confirms that the fourth-order, symmetry-preserving method is more accurate than the second-order method. With 48 or more grid points in the wall normal direction, the root-mean-square of the fluctuating velocity obtained by the fourth-order method is in close agreement with that computed by Kim *et al.* (1987) for $y^+ > 20$ (Figure 7 shows this only for y^+ up to 40; yet, the agreement is also excellent for $y^+ > 40$). In the vicinity of the wall ($y^+ < 20$), the velocity fluctuations of the fourth-order simulation method

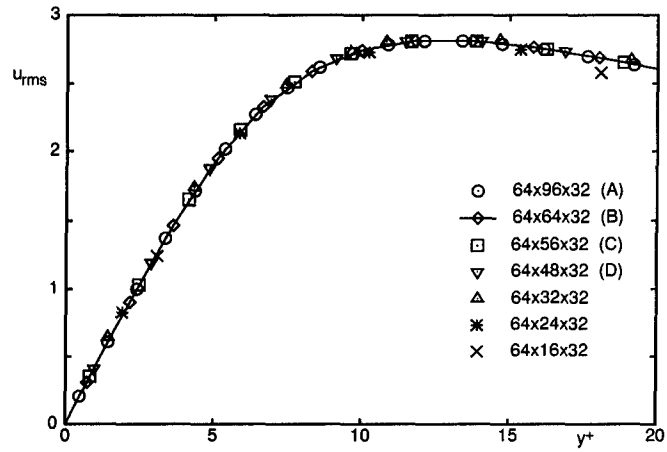

Figure 5. The root-mean-square velocity fluctuations normalized by the wall shear velocity as function of the wall coordinate y^+ on various grids for $y^+ \leq 20$. The markers correspond to the results obtained in the grid points. The solution on grid B is also represented by a continuous line.

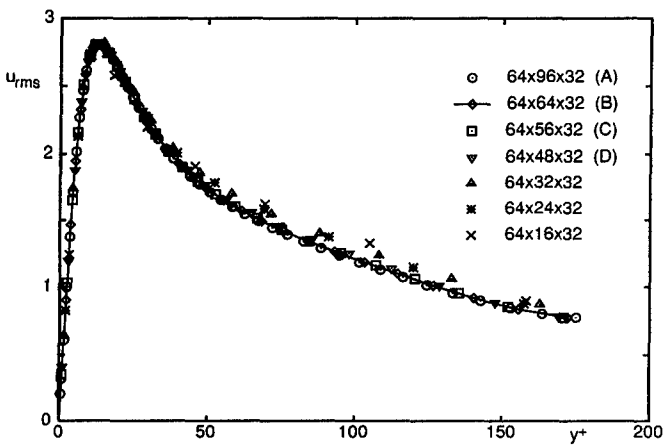

Figure 6. The root-mean-square velocity fluctuations normalized by the wall shear velocity for $y^+ \leq 200$ on various grids.

fit the experiment data nicely, even up to very coarse grids with only 24 grid points in the wall-normal direction. However, the turbulence intensity

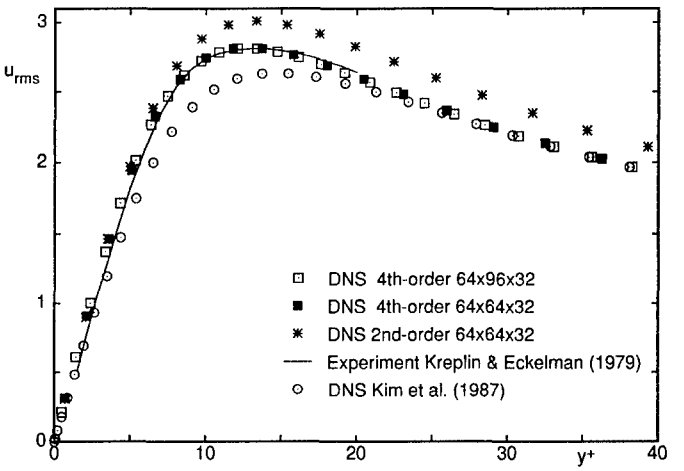

Figure 7. Comparison of the mean-square of the streamwise fluctuating velocity as function of y^+.

in the sublayer ($0 < y^+ < 5$) predicted by the simulations is higher than that in the experiment. According to the fourth-order simulation the root-mean-square approaches the wall like $u_{\rm rms} \approx 0.38 y^+$ ($N_y = 64$). The exact value of this slope is hard to pin-point experimentally. Hanratty *et al.* (1977) have fitted experimental data of several investigators, and thus came to 0.3. Most direct numerical simulations yield higher values. Kim *et al.* (1987) and Gilbert and Kleiser (1991) have found slopes of 0.3637 and 0.3824 respectively, which is in close agreement with the present findings.

So, in conclusion, the results of the fourth-order symmetry-preserving discretization agree better with the available reference data than those of its second-order counterpart, and with the fourth-order method a $64 \times 64 \times 32$ grid suffices to perform an accurate DNS of a turbulent channel flow at Re=5,600.

References

Antonopoulos-Domis, M. (1981) Large-eddy simulation of a passive scalar in isotropic turbulence. J. Fluid Mech. **104**, 55–79

Dean, R. B. (1978) Reynolds number dependence of skin friction and other bulk flow variables in two-dimensional rectangular duct flow. J. Fluids Engng. **100**, 215–223

Ducros, F., Laporte, F., Soulères, T., Guinot, V. Moinat, P. and Caruelle, B. (2000) High-order fluxes for conservative skew-symmetric-like schemes in structured meshes: application to compressible flows. J. Comp. Phys. **161**, 114–139

Gilbert, N. and Kleiser, L. (1991) Turbulence model testing with the aid of direct numerical simulation results. Proc. Turb. Shear Flows 8, Paper 26-1

Hanratty, T. J., Chorn, L. G. and Hatziavramidis, D. T. (1977) Turbulent fluctuations in the viscous wall region for Newtonian and drag reducing fluids. Phys. Fluids **20**, S112

Harlow, F. H. and Welsh, J. E. (1965) Numerical calculation of time-dependent viscous incompressible flow of fluid with free surface. Phys. Fluids **8**, 2182–2189

Hyman, J. M., Knapp, R. J., and Scovel, J. C. (1992) High order finite volume approximations of differential operators on nonuniform grids. Physica D **60**, 112–138

Kim, J., Moin, P. and Moser, R. (1987) Turbulence statistics in fully developed channel flow at low Reynolds number. J. Fluid Mech. **177**, 133–166

Kreplin, H. P. and Eckelmann, H. (1979) Behavior of the three fluctuating velocity components in the wall region of a turbulent channel flow. Phys. Fluids **22**, 1233–1239

Kuroda, A., Kasagi, N. and Hirata, M. (1995) Direct numerical simulation of turbulent plane Couette-Poisseuille flows: effect of mean shear rate on the near-wall turbulence structures. In: F. Durst et al. (Eds.) Proc Turb. Shear Flows, Springer-Verlag, Berlin, 241–257

Manteufel, T. A. and White, Jr., A.B. (1986) The numerical solution of second-order boundary value problems on nonuniform meshes. Math. of Comp. **47**, 511–535

Morinishi, Y., Lund, T. S., Vasilyev, O. V. and Moin, P. (1998) Fully conservative higher order finite difference schemes for incompressible flow. J. Comp. Phys. **143**, 90–124

Twerda, A. (2000) Advanced computational methods for complex flow simulation. Delft University of Technology, PhD thesis.

Vasilyev, O .V. (2000) High order finite difference schemes on non-uniform meshes with good conservation properties. J. Comp. Phys. **157**, 746–761

Verstappen, R. W. C. P. and Veldman, A. E. P. (1997) Direct numerical simulation of turbulence at lower costs. J. Engng. Math. **32**, 143–159

Verstappen, R. W. C. P. and Veldman, A. E. P. (1998) Spectro-consistent discretization of Navier-Stokes: a challenge to RANS and LES. J. Engng. Math. **34**, 163–179

Verstappen, R. W. C. P. and Veldman, A. E. P. (2002) Symmetry-preserving discretization of turbulent flow, submitted to J. Comp. Phys.